

Quantum Adversarial Learning for Kernel Methods

Giuseppe Montalbano^{1,*} and Leonardo Banchi^{2,3,†}

¹*Ca' Foscari Challenge School, University Ca' Foscari, Dossoduro 3246, Venezia, 30123, Italy.*

²*Department of Physics and Astronomy, University of Florence,
via G. Sansone 1, I-50019 Sesto Fiorentino (FI), Italy*

³*INFN Sezione di Firenze, via G. Sansone 1, I-50019, Sesto Fiorentino (FI), Italy*

(Dated: April 10, 2024)

We show that hybrid quantum classifiers based on quantum kernel methods and support vector machines are vulnerable against adversarial attacks, namely small engineered perturbations of the input data can deceive the classifier into predicting the wrong result. Nonetheless, we also show that simple defence strategies based on data augmentation with a few crafted perturbations can make the classifier robust against new attacks. Our results find applications in security-critical learning problems and in mitigating the effect of some forms of quantum noise, since the attacker can also be understood as part of the surrounding environment.

1. Introduction

With the advance of artificial intelligence and its adoption in strategic, safety-critical and healthcare applications, it has become essential to study the possible vulnerabilities that affect the different types of algorithms, and to develop appropriate countermeasures. Because of this, the possibility of deceiving machine learning algorithms by means of intentionally crafted data as well as the design of proper defense strategies has been investigated quite actively in classical machine learning, giving rise to the research field of adversarial machine learning (Biggio and Roli 2018).

Adversarial machine learning studies many ways of attacking and defending machine learning algorithms with different kinds of attacks, that can be characterized based on three aspects: i) the *time* when the attack is performed, and whether the algorithm or the model is attacked; ii) the *amount of information* needed to perform the attack, e.g. in so called white-box attacks we have complete details about the algorithm and the data, in contrast to black-box attacks where the algorithm and the model is unknown to the attacker; iii) the *goals of the attack*, e.g. an untargeted attack, when the attacker wants to cause just a wrong behaviour, or a targeted attack, when they want to achieve a specific result. Input data that are purposely crafted by an attacker to induce the model to make mistakes are generally called adversarial examples or adversarial samples. It has been shown that, in some cases, these adversarial examples can take the form of imperceptibly small perturbations to real input data, such as making a human-invisible change to pixels of an image (Szegedy *et al.* 2014).

Given the remarkable progresses in quantum computing hardware, different machine learning algorithms and techniques have been adapted to exploit the computation capabilities offered by these systems, giving rise to

the field of Quantum Machine Learning (QML). However, due to the limitations of current devices, such an adaptation often requires a significant algorithmic redesign to streamline the number of operations done in quantum device itself. Therefore, it is not always trivial to adapt tricks and results from the classical literature to the quantum case. Two popular quantum machine learning algorithms are based on Quantum Neural Networks (QNN) and Quantum Kernel Methods (QKM), see e.g. (Schuld *et al.* 2015). The vulnerability of quantum neural networks against adversarial attacks and the development of defence strategies have been investigated both theoretically (Lu *et al.* 2020; Liu and Wittek 2020) and experimentally (Ren *et al.* 2022).

In this work we show the vulnerability of quantum kernel methods against similar attacks, and develop a simple defence strategies based on data augmentation with the crafted adversarial samples. We focus on binary classification tasks for classical data, though similar considerations can be done for the classification of quantum data, which has different applications (Gebhart *et al.* 2023). In the latter case, perturbations needs to be directly applied to the quantum state. Our results are supported by both analytical arguments and extensive numerical simulations, performed using the Qiskit library (Qiskit contributors 2023).

Our results find application in safety-critical learning problems, but also for the development of more robust learning techniques against quantum noise. Indeed, a subset of the unavoidable errors in current quantum devices can be understood as a perturbation in the inputs. While we cannot fix general hardware errors without sophisticated error correction or mitigation techniques, we can make the model more robust against input perturbations, and, as a result, against fluctuations in the parameters of the encoding gates. To show that by developing robust algorithms against adversarial inputs, we can also mitigate the effect of some hardware noise, we have performed a proof-of-principle experiment on a real device, using the IBM Quantum Platform.

* giu.montalbano@gmail.com

† leonardo.banchi@unifi.it

2. Background

In this section we provide a mathematical introduction to adversarial learning and kernel methods.

2.1. Quantum adversarial machine learning

Let $X \subset \mathbb{R}^d$ and Y denote, respectively, the space of classical inputs and discrete labels. In supervised learning tasks on classical data, we have access to a training dataset $D := \{x_i, y_i\}_{i=1}^M$ with M pairs, where $x_i \in X$ are input vectors and $y_i \in Y$ are the associated labels. The input vectors and the labels are related by some unknown function $f : X \mapsto Y$. The goal of the supervised learning task we consider is to train a model $h(\cdot, \theta) : X \mapsto Y$ to approximate f , where the vector θ defines the model parameters, belonging to some appropriate subset of \mathbb{R}^N .

To train the model we define a loss function $\mathcal{L}(h(\cdot, \theta), \cdot) : (X \times Y) \mapsto \mathbb{R}$ that introduces a penalty whenever the predicted label is different from the true one, i.e. $h(x, \theta) \neq f(x)$. We then define the empirical loss

$$\mathcal{L}(D, \theta) = \frac{1}{M} \sum_{i=1}^M \mathcal{L}(h(x_i, \theta), y_i), \quad (1)$$

which measures, on average, how well the model approximates f on D . The training problem can be formulated as a minimization problem:

$$\theta_{\text{opt}} = \arg \min_{\theta} \mathcal{L}(D, \theta). \quad (2)$$

In kernel methods the above optimization problem is convex and therefore one is guaranteed that the optimal parameters θ_{opt} define a global optimum. This is a strong theoretical advantage of kernel-based QML algorithms compared to QNNs. Once the training process is completed, namely the above optimization is solved, the model is evaluated on a test dataset of unseen input vectors to check its generalization capabilities.

The type of attack that we consider in this study belongs to the category of white-box untargeted attacks, applied against the model of a quantum classifier. In this scenario, the technique to generate an adversarial sample starting from a true sample x_i consists on leveraging the same loss function used during the training of the model, though in this case the parameters θ are kept fixed at their optimal value θ_{opt} found during training, and we maximize over the input space:

$$\delta_{i,\text{adv}} = \arg \max_{\delta \in \Delta} \mathcal{L}(h(x_i + \delta, \theta_{\text{opt}}), y_i), \quad (3)$$

where Δ represents a limited region of the input space where to look for a solution, in order to keep the perturbation small.

2.2. Quantum-enhanced support vector machines

Machine learning techniques based on kernel methods are a family of techniques that builds on the idea of using a particular measure to evaluate the similarity between vectors in some appropriate Hilbert space with the objective to solve some task (Schuld and Petruccione 2021). In this work we focus on binary classification via Support Vector Machines (SVM) (Cristianini and Shawe-Taylor 2000) where training consists in finding a decision hypersurface on a Hilbert space, called *feature space*, and the classification is done by checking on which side of the plane the input belongs. QML algorithms based on kernel methods and SVM have gained significant attention as a potential candidate for achieving a possible quantum advantage over classic algorithms (Liu *et al.* 2021).

For simplicity we focus on binary classification problems with $Y = \{+1, -1\}$. A nonlinear SVM classifier makes decisions about the class of an input sample using an optimal hypersurface in the input space, which is mapped into a hyperplane in the feature space. The latter is defined as

$$\langle w, \phi(x) \rangle + b = 0, \quad (4)$$

where $\phi(x)$ is the *embedding* function that maps the input to the feature space. The optimal hyperplane is selected by solving a quadratic programming, a convex optimization problem with inequality constraints, described in its dual problem formulation as follows:

$$\max_{\alpha} \left[\sum_{i=1}^M \alpha_i - \frac{1}{2} \sum_{i,j=1}^M y_i y_j \alpha_i \alpha_j k(x_i, x_j) \right], \quad (5)$$

with constraints $\sum_{i=1}^M \alpha_i y_i = 0$ and $0 \leq \alpha_i \leq C$ for $i = 1 \dots M$, where C is an hyper-parameter used as a penalty weight to address samples in the training dataset that would not allow a linear separation in the considered feature space. The kernel

$$k(x_i, x_j) = \langle \phi(x_i), \phi(x_j) \rangle, \quad (6)$$

is the (euclidean) inner product between two feature vectors, obtained via an embedding function ϕ . The convex optimization problem in Eq. (5) can be solved with open-source libraries (Chang and Lin 2011) with polynomial complexity in M . From the solution of the dual problem, it is possible to show that $w = \sum_{i=1}^M y_i \alpha_i \phi(x_i)$, with a related expression for b (see below). Once the optimal hypersurface has been found, the nonlinear SVM classifier predicts the label of an input sample based on the sign of the decision function $f(x)$:

$$f(x) = \langle w, \phi(x) \rangle + b = \sum_{i=1}^M \left[\alpha_i y_i k(x_i, x) + \frac{y_i - \sum_{j=1}^M \alpha_j y_j k(x_i, x_j)}{M} \right]. \quad (7)$$

When $f(x) \geq 0$ the classifier predicts a label +1, otherwise it predicts a label -1. We observe that in the dual formulation, both the training and test processes, Eqs. (2) and (7), do not require any evaluation in the feature space with the exception of the kernel (6), while the direct optimization of w in the primal formulation might be complex for very large feature spaces.

Quantum circuits can be exploited to define a feature space with a dimension that increases exponentially with the number of qubits n , which may allow an easier separation of inputs with different labels. Let $U(x)$ be a unitary circuit applied to an initial state $|0^n\rangle$ to produce $|\phi(x)\rangle = U(x)|0^n\rangle$. Following (Schuld and Petruccione 2021) we define the encoding feature map $\phi: \mathbb{R}^d \mapsto \mathcal{F}$ as the function mapping each input sample $x \in \mathbb{R}^d$ to the density matrix $\phi(x) = |\phi(x)\rangle\langle\phi(x)| =: \rho(x)$, where \mathcal{F} is the space of density matrices of size $2^n \times 2^n$, equipped with the Hilbert-Schmidt inner product $\langle\rho, \sigma\rangle_{\mathcal{F}} = \text{Tr}(\rho^\dagger\sigma)$ for $\rho, \sigma \in \mathcal{F}$. With these definitions the kernel (6)

$$k(x_1, x_2) = \text{Tr}(\rho(x_2)\rho(x_1)) = |\langle\phi(x_2)|\phi(x_1)\rangle|^2,$$

is nothing but the fidelity between two quantum state embeddings. Although such embeddings map the inputs onto a space that grows exponentially with the number of qubits, by exploiting the kernel trick, we only need to know how to evaluate the kernel values between feature vectors corresponding to samples mapped from the input dataset. This allows us to avoid optimization problems in a huge Hilbert space, and to work directly with the space of the training dataset that, having a lower dimension, is easier to manipulate.

A Quantum-enhanced Support Vector Machine (QSVM) is a hybrid classical-quantum algorithm that exploits a quantum system to compute the quantum kernel values and uses a classical SVM algorithm to determine the optimal decision hypersurface. There are different techniques to estimate the quantum kernel by means on a quantum computer. Examples include a technique commonly referred to as Quantum Kernel Estimation (QKE) (Liu *et al.* 2021; Havlíček *et al.* 2019), which consists in concatenating the two circuits, followed by an estimation of the probability to measure all qubits in the state $|0\rangle$. Accordingly, for a single kernel value, we have to repeat the measurement many times in order to obtain a good estimation. For embedding circuits with many layers, alternative circuits such as the swap test might be more appropriate (Schuld and Petruccione 2021).

The quantum embedding circuit that we use to encode input data into quantum states completely describes the associated quantum kernel and therefore characterizes the performance achievable by the SVM classifier. A general goal is, therefore, to look for a kernel that guarantees the best performance and that best fits the dataset at hand. Since the optimal kernel is unknown, we use the kernel alignment technique described in appendix A to optimize the quantum circuit, and hence the kernel.

3. Adversarial Learning on Quantum-Enhanced Support Vector Machines

Following the general scheme introduced in Sec. 2.1, we now introduce a technique to perturbate a legitimate input sample to deceive a previously trained QSVM classifier. In addition to the general concepts described previously, we have to consider a couple of basic aspects:

- Knowing the principles on which a SVM builds on, the goal of the attacker is to generate adversarial perturbations to legitimate samples, so that the resulting feature vectors (density matrices) are located on the other side of the decision hypersurface, with respect to the unperturbed ones. This type of attack is referred to in literature as Evasion Attack (Li *et al.* 2022).
- The perturbations to the original samples should be as “light” as possible, so we would like to keep the distance between the original sample x and its modified version x_{adv} small. A possible way to evaluate this distance, is to use the euclidean distance $\|x - x_{\text{adv}}\|_2$.

To enforce these two constraints simultaneously, we may focus on Eq. (3) and add a penalty term $\|x - x_{\text{adv}}\|^2$, in place of the hard constraint $\delta \in \Delta$. Assuming that $x_{\text{adv},i} = x_i + \delta_i$ with a small δ_i , we find

$$\delta_{i,\text{adv}} = \arg \max_{\delta_i} \mathcal{L}(f(x_i + \delta_i), y_i) - \frac{\|\delta_i\|^2}{2\eta}, \quad (8)$$

$$\approx \arg \max_{\delta_i} \nabla_x \mathcal{L}(f(x_i), y_i) \cdot \delta_i - \frac{\|\delta_i\|^2}{2\eta}, \quad (9)$$

where η is a positive parameter to tune the strength of the penalty term. In SVM \mathcal{L} is the hinge loss $\mathcal{L}(f(x), y) = \max\{0, 1 - yf(x)\}$, hence the above problem has the following solution

$$\delta_{i,\text{adv}} \approx -\eta y_i \nabla_x f(x_i), \quad (10)$$

which can be interpreted as a single gradient step with learning rate η . Geometrically, the value of $\nabla_x f$ is a vector normal to intersection line between the hyperplane tangent to the hypersurface defined by the decision function $f(x)$ at x_i and the hyperplane $z=0$, see Fig. 1. Note also that the hinge loss is analytic away of the decision hypersurface. Leveraging these observations, we can implement an iterative procedure that starts from an initial point x_i and shifts that point toward the separating hypersurface, using the gradient of the decision function as the direction to update the point at each step. By repeating the above procedure, the adversarial perturbation at the t -th iteration satisfies

$$x_{i,\text{adv}}^{t+1} = x_{i,\text{adv}}^t - \eta_i^t y_i \nabla_x f(x_{i,\text{adv}}^t), \quad (11)$$

with $x_{i,\text{adv}}^0 = x_i$ and where η_i^t is an adaptive learning rate – in the simplest case $\eta_i^t \equiv \eta$. The iteration is stopped

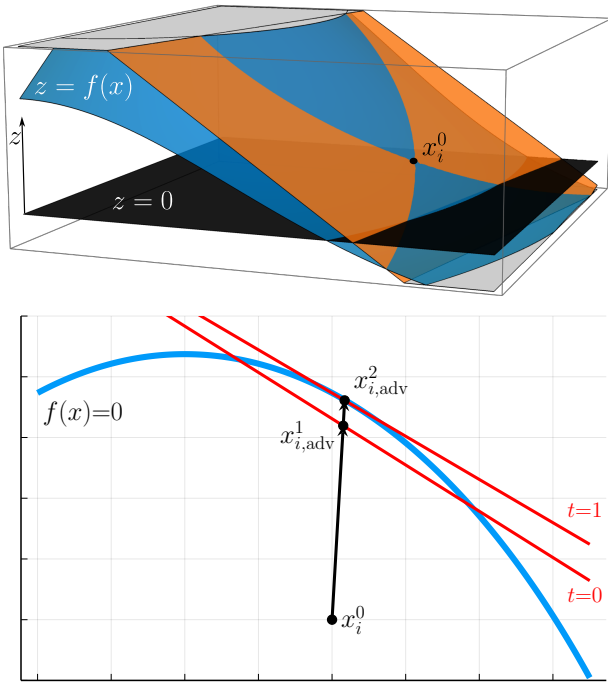


FIG. 1. (top) Three dimensional representation of the decision function f (blue) for a two-dimensional input x and an extra axis z , together with the tangent plane near x_i^0 (orange). (bottom) The intersection of the above surfaces with the $z = 0$ plane (in black in the top figure), together with two steps of the iteration described by Eqs. (11) and (13). The blue line is the decision hypersurface $f(x) = 0$, while the orange lines are the approximations of the hypersurface at iterations $t = 0$ and $t = 1$, using hyperplanes – that for $t = 0$ is a projection of the orange hyperplane from the top figure.

once $\rho(x_{i,\text{adv}}^t)$ is located on the other side of the decision hypersurface, or the maximum number of iterations is reached. The latter must be kept small to guarantee a small $\|x_i - x_{i,\text{adv}}\|$.

A better iterative technique can be defined by exploiting the geometrical structure of SVMs. To clarify this, we start with linear SVM, where $\phi(x) \equiv x$ and the decision hypersurface (4) can be written as a hyperplane $f(x) = w^T x + b = 0$. The vector w is normal to the hyperplane, and $|f(x_i)|/\|w\|$ is the distance between a general point x_i and the hyperplane. Leveraging this observation, to project a point into the plane we should add a perturbation along the orthogonal direction, identified by the normalized vector $w/\|w\|$, with a strength given by the distance. This results in

$$\delta_i = -\frac{w}{\|w\|} \frac{|f(x_i)|}{\|w\|}. \quad (12)$$

In the general case, where the embedding map ϕ is non-linear, $f(x) = 0$ identifies a hypersurface, which can be approximated as a hyperplane around a certain point x_i as $f(x_i + \delta_i) \approx f(x_i) + \nabla_x f(x_i)^T \delta_i$, as shown in Fig. 1. Therefore, the vector w from the previous analysis can be

| | Training set | Test set | Total |
|--------|--------------|----------|-------|
| Hand | 245 | 45 | 290 |
| Breast | 255 | 55 | 310 |
| Total | 500 | 100 | 600 |

TABLE I. Composition of the training and test datasets.

replaced with the gradient of f . Combining this intuition with Eq. (12), in the non-linear case the formula to find an adversarial perturbation becomes equivalent to the gradient step (10), but with an *adaptive* learning rate (Li *et al.* 2022)

$$\eta_i^t = \frac{|f(x_{i,\text{adv}}^t)|}{\|\nabla_x f(x_{i,\text{adv}}^t)\|^2}. \quad (13)$$

Since the approximated decision hyperplane changes during the iteration, due to the curvature of the hypersurface, the above procedure must be repeated multiple times, as in (11). A pictorial representation of this iteration is shown in Fig. 1. When $x_{i,\text{adv}}^t$ approaches the decision hypersurface, η_i^t can get very small. In that case, we may empirically replace the adaptive learning rate (13) with a larger constant η .

From the above analysis it is clear that the best way to generate adversarial samples is to start either from inputs x_i with $|f(x_i)| \approx 0$, which are close to the hypersurface and can switch side with few gradient steps, or from inputs with a large gradient. When quantum kernels are built via deep quantum circuits, then from the kernel concentration phenomenon (Thanasilp *et al.* 2022), we can expect that $|f(x_i)| \approx 0$ for a large number of inputs, making the generation of adversarial samples easier.

This technique to generate adversarial samples builds on the assumption that we can compute the gradient of f , which, thanks to the analytic expression Eq. (7), requires the ability to compute the gradient of the quantum kernel. Since the kernel depends linearly on the state $\rho(x)$, it is possible to use techniques such as the parameter-shift rule (Schuld and Petruccione 2021; Mitarai *et al.* 2018; Banchi and Crooks 2021) to express the ℓ th component of the gradient as

$$\partial_{x_\ell} f(x) = \sum_{i=1}^M \alpha_i y_i [k(x_i, x + \pi_\ell) - k(x_i, x - \pi_\ell)], \quad (14)$$

where the vector $\pi_\ell \in \mathbb{R}^d$ has components $(\pi_\ell)_i = \frac{\pi}{4} \delta_{i,\ell}$. When the embedding circuit contains gates that cannot be simply expressed via Pauli rotations, it is necessary to use extensions such as the stochastic parameter-shift rule (Banchi and Crooks 2021).

4. Results

In our numerical study, we use one of the datasets exploited in the work on adversarial training with quantum



FIG. 2. Some samples from the training and test dataset.

neural networks (Ren *et al.* 2022), so we can compare the results. That dataset is publicly available and consists of images from the Medical MNIST, a collection of standardized biomedical images. Some examples are shown in Fig. 2. In the experiments we use a subset composed of 600 monochromatic images, consisting of Magnetic Resonance Imaging data of two classes: hand and breast, divided as in Table I. The images are scaled to the resolution of 16 by 16 pixels and then normalized.

After some preliminary experiments we decided to use a quantum embedding circuit with a structure very similar to the one used in (Ren *et al.* 2022): we designed a quantum circuit with the same number of qubits, 10, to efficiently map the input data into a quantum state, using some tunable parameters and some entangling layers, implemented with CNOT gates.

We map the 16×16 pixels of each image in 10 qubits using three blocks of angle encoding layers: i) 8 alternating layers of Rx and Rz gates; ii) 12 alternating layers of Rx and Rz gates; iii) 6 alternating layers of Rx and Rz gates. Two layers of CNOT gates between nearest qubits are added after each block of angle encoding gates to create entanglement. Before data encoding, each input sample is extended with four zero components so to map exactly into the 260 angle encoding gates. To define a tunable quantum embedding we also introduce 30 variational parameters θ_i with $i = 0 \dots 29$. To reduce the total number of angle encoding gates in the quantum circuit, these parameters are summed up to the first 30 components of the input data x_i and encoded in the first three layers of gates. This is equivalent to consider each of the first three layers of gates as actually composed of two layers of rotation gates each, where input data and tunable parameters are encoded into dedicated angle encoding gates. From now on, we will call such an encoding circuit the *large feature map*.

However, such a deep quantum circuit is challenging in terms of both implementability with NISQ hardware and trainability of the parameters. For these reasons, we decided to work also with a more compact circuit, shown in Fig. 3, that we call *compact feature map*. By means of a Principal Component Analysis (PCA) carried on the training data we identified that with a compression of the data space from a dimension of 256 to 80 it is still possible to convey more than 94% of the information, as measured by the cumulative sum of the variance explained by the selected components. We also introduce 20 tunable angles θ_i with $i = 0 \dots 19$ and encode them together with the input data x_i , in the first two layers of the quantum circuit. This choice should reduce the

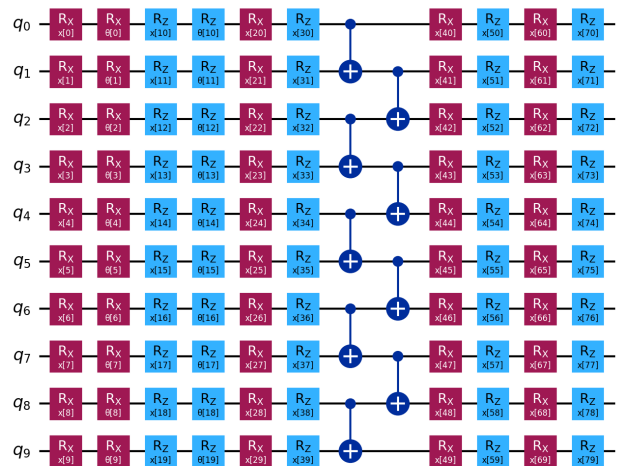


FIG. 3. Compact feature map for compressed input data, reduced via PCA transformation. The embedding circuit consists of 80 angle encoding gates, loading the classical vector $(x[0], \dots, x[79])$ into the quantum register, and 20 parametric gates, with parameters $(\theta[0], \dots, \theta[19])$. Note that the parametric gates can be combined with the encoding gates to reduce the circuit depth, and further merged via the Euler angle decomposition.

expressibility of the associated feature map, which is a necessary condition to avoid concentration of quantum kernel values phenomenon (Thanasilp *et al.* 2022), an obstacle to trainability of kernel methods.

4.1. Standard training

We carried out the kernel alignment procedure, described in appendix A, to optimize the tunable parameters of the quantum feature maps. The decay of the cross-entropy loss as the number of iterations increases is shown in Fig. 4, for both the large and compact quantum embeddings. The optimization of the parameters was quite computationally heavy. We performed the kernel alignment with respect to the full training dataset, which required the evaluation of the quantum circuit many times to compute a 500 by 500 kernel matrix needed in each iteration step of the optimization procedure. Both circuits have been initialized with random parameters and optimized with SPSA. More details are provided in appendix B.

Once the parameters of the quantum embedding circuits are optimized with the kernel alignment procedure, we can observe that the entries of the kernel matrices, shown in Fig. 5, are quite distributed within the interval $[0, 1]$ for both quantum embeddings circuits. This means that we are far away from a situation where we can encounter the exponential concentration phenomenon, where we would expect to find large areas of the kernel matrix concentrated around a fix value, with an associ-

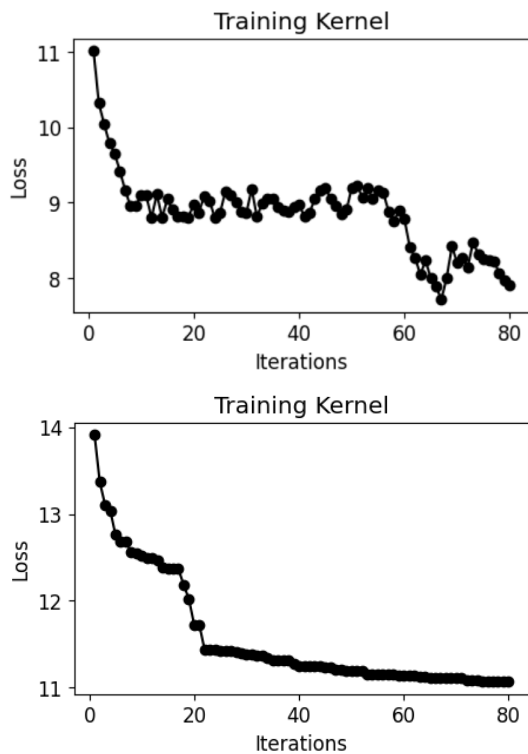


FIG. 4. Kernel-target alignment of both large (top figure) and compact (bottom figure) feature maps. The Cross-entropy loss was employed for the min-max optimization.

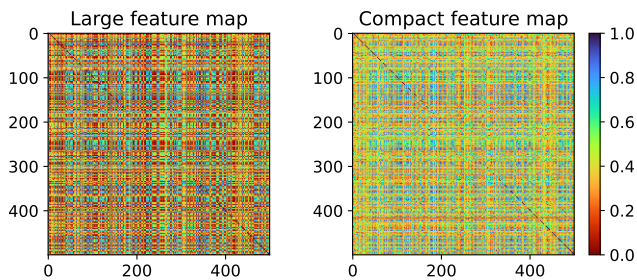


FIG. 5. Kernel matrices of the training dataset, after the kernel alignment procedure, using either the large (left figure) or the compact (right figure) feature maps.

ated image that takes the same color in large continuous zones above and below the diagonal.

The kernel matrices computed by means of the larger feature map contain several “spots” where the kernel value is zero. This is probably because the kernel alignment procedure was interrupted after 80 steps, when the loss function was still decreasing. This is a symptom that the kernel alignment procedure was not completed and that there is still margin to optimize the parameters of that quantum embedding circuit.

After computing the 500×500 kernel matrix, we can fit a classical SVM algorithm on the training dataset, exploiting the kernel computed via a quantum circuit. The performance of the trained SVM models is shown in

| | Large feature map | Compact feature map |
|-------------------|-------------------|---------------------|
| Training accuracy | 1.00 | 1.00 |
| Test accuracy | 0.99 | 1.00 |
| F1-score (test) | 0.99 | 1.00 |

TABLE II. Summary of the performance of trained QSVM models.

| | | Large feature map | | Compact feature map | |
|------|--------|-------------------|--------|---------------------|--------|
| | | Hand | Breast | Hand | Breast |
| True | Hand | 45 | 0 | 45 | 0 |
| | Breast | 1 | 54 | 0 | 55 |

TABLE III. Confusion matrix between true (T) and predicted (P) labels, evaluated on the test dataset for the trained QSVM based on the large (left) and compact (right) feature maps.

Table II, while the confusion matrix is illustrated in Table. III. Both SVM classifiers have been trained adopting a K-fold cross-validation strategy with $K = 5$ to select the hyper-parameter C , with found optimal value $C = 1$.

4.2. Adversarial training

After training the QSVM, we produce adversarial images by following the procedure outlined in Sec. 3. Some examples are shown in Fig. 6. All the produced adversarial examples deceive the QSVM classifier by construction. In most cases, a human eye can still recognise an adversarial hand as a hand, and an adversarial breast as a breast. However, in a few examples, e.g. the sixth, ninth and tenth columns in Fig. 6, the algorithm smoothly transform a hand into a breast, signalling that the algorithm introduced a large perturbation to the image.

We generate 50 adversarial images for both large and compact embeddings and randomly distribute them using a stratified approach into two sets, one with 41 samples and one with the remaining 9 samples. The larger set is then joined to the original training samples, while the smaller one to the test samples.

As expected, checking the behaviour of the trained QSVM classifier on the extended test dataset reveals a decrease of the performance. As detailed in Table. IV all the perturbed examples are wrongly classified. This highlights the vulnerability of the previously trained QSVM to evasion attacks.

The next step is to verify whether the adversarial training technique results effective for the development of QSVM classifiers robust to evasion attacks, in analogy to what was previously observed for the QNN classifier (Ren *et al.* 2022).

We carry on a new training of the QSVM considering the modified training dataset, now extended with 41 adversarial examples. We keep the parameters of the quantum embedding fixed to the values we have optimized before, via the quantum alignment. Also in this case we adopted a K-fold cross-validation strategy with $K=5$ to

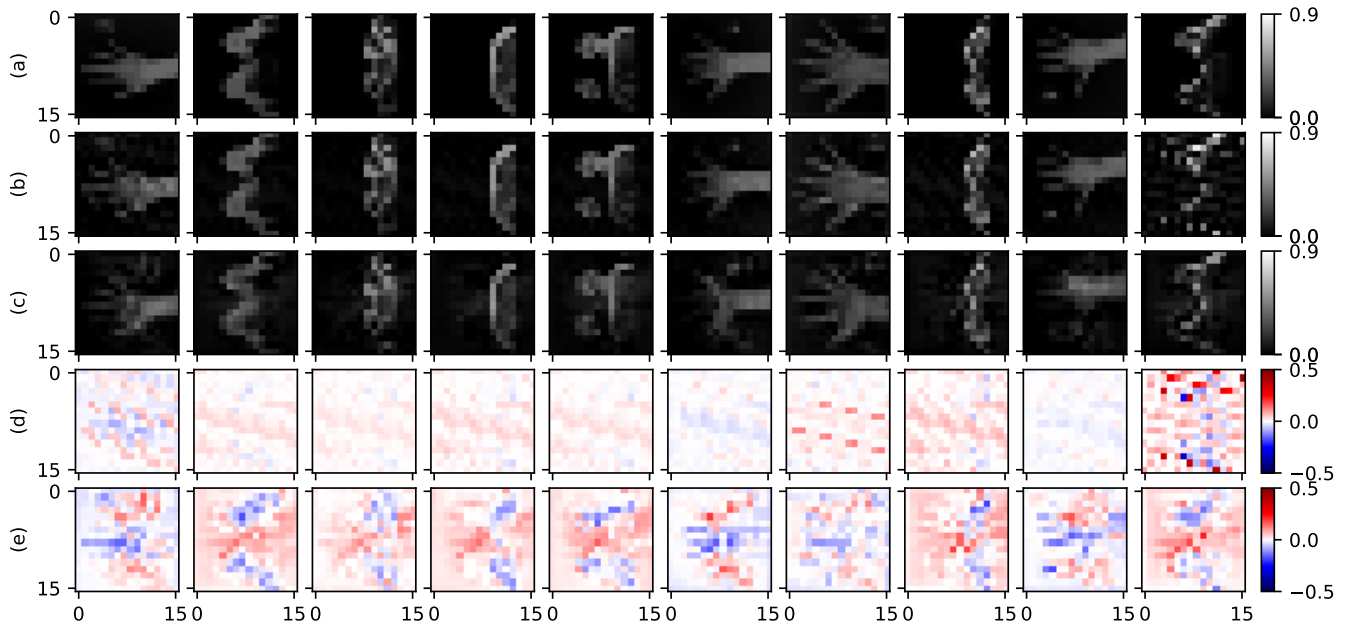


FIG. 6. Original and adversarial images arranged into a grid. In each column, (a) is the original sample, (b) and (c) the corresponding adversarial examples for the large and compact feature map, respectively, (d) and (e) show the perturbation that, summed up to the original image, generates (b) and (c), respectively.

| | Large feature map | Compact feature map |
|-----------------|-------------------|---------------------|
| Test accuracy | 0.91 | 0.92 |
| F1-score (test) | 0.92 | 0.92 |

| | | Large feature map | | Compact feature map | |
|------|--------|-------------------|--------|---------------------|--------|
| | | Hand | Breast | Hand | Breast |
| True | Hand | 45 | 4 | 45 | 4 |
| | Breast | 6 | 54 | 5 | 55 |

TABLE IV. Summary of the performance of trained QSVM models on the test set extended with adversarial examples, together with the confusion matrix between true and predicted labels, evaluated on the test dataset extended with 9 adversarial samples (4 'hand' and 5 'breast') for the trained QSVM based on the large and compact feature maps.

identify the best hyper-parameter C . The result is $C=1.0$ for the large embedding and $C=2.0$ for the compact one. After adversarial training with both models, we observe a significant increase of the performance, as detailed in Table. V.

Looking at these numerical results we can affirm that the adversarial training technique is effective for the development of QSVM classifiers robust to evasion attacks.

4.3. Kernel computation on a real quantum system

In this section we describe a proof-of-principle experiment on a real quantum hardware. We consider the adversarially trained QSVM model based on the compact embedding, and use a real quantum hardware to estimate the quantum kernel values required to predict the labels of previously unseen samples. For this experiment we used a quantum computer available within the open plan service of the *IBM Quantum Platform*. Because of the limitations we had on the resources available, we leveraged the quantum hardware to predict the label of one

sample only. Nevertheless, the procedure is general and valid to perform computations for any number of samples.

To reduce computation time on the quantum system and mitigate issues associated with noise, we transpiled the circuit considering the specificities of the real hardware. Among the quantum systems accessible via the *IBM Quantum Platform*, we selected the *ibm_kyoto* backend, a quantum system based on the quantum processor family *Eagle*, with 127 qubits and a quantum volume of 128. The final circuit is characterized by 77 layers of gates.

To estimate the quantum kernel values on the real quantum hardware we used the `Sampler` primitive from Qiskit (Qiskit contributors 2023), configured to carry on 1024 shots for each circuit. The quantum processor evaluated 553984 (1024×541) circuits and took 8 minutes approximately. Once the job was completed and the results provided back, we populated the kernel matrix.

Finally, we used the nonlinear SVM previously trained to predict the label of the sample. Our experiment terminated successfully: the adversarial example was classified

| | Large feature map | Compact feature map |
|-------------------|-------------------|---------------------|
| Training accuracy | 0.99 | 0.99 |
| Test accuracy | 1.00 | 1.00 |
| F1-score (test) | 1.00 | 1.00 |

| | | Large feature map | | Compact feature map | |
|------|--------|-------------------|--------|---------------------|--------|
| | | Hand | Breast | Hand | Breast |
| True | Hand | 49 | 0 | 49 | 0 |
| | Breast | 0 | 60 | 0 | 60 |

TABLE V. Summary of the performance of QSVM models after adversarial training, together with the confusion matrix between true and predicted labels, evaluated on the extended test dataset after adversarial training.

correctly by the quantum-enhanced SVM, trained adopting the adversarial training technique and evaluating the quantum kernel on a real quantum processor.

This proof-of-principle experiments showcase the possibility that adversarial training makes the predictions of a QSVM model more robust, not only against perturbations of the inputs, but also against hardware noise (Banchi 2022).

5. Conclusions

The numerical results from our simulations clearly show that quantum classifiers based on kernel methods, like quantum-enhanced SVM, are vulnerable to the evasion attacks, similarly to what happens with Quantum Neural Networks (Ren *et al.* 2022). The well-developed mathematical theory behind SVM allows us to have a simple geometrical picture to understand when this is possible. The narrower the SVM margin is, the smaller is the perturbation that an attacker needs to generate, and so the higher is the possibility to disguise an adversarial example as a legitimate sample. Due to the kernel concentration phenomenon (Thanasilp *et al.* 2022), this possibility is quite likely with complex quantum embeddings.

We have also shown how to make the prediction robust against such attacks by using adversarial training: adding adversarial examples to the training dataset makes the SVM algorithm to select an optimal decision hypersurface with better generalization and, hence, better distinguishing capabilities. In other terms, adversarial training forces the decision hypersurface to position itself in the Hilbert space in such a way to achieve the largest margin. While from the kernel concentration phenomenon we may expect, for complex embeddings, a high success probability in carrying out evasion attacks, the robustness of adversarial training in such regime is less clear and needs further studies. Indeed, the concentration depends also on the expressibility induced by the input dataset. On one hand we would like to enlarge the legitimate training dataset with as many adversarial examples as possible, so to improve the robustness of the classifier, but on the other hand such an increase induces an increase in the input randomness, which might make kernel values even more concentrated and, as such, more difficult to evaluate experimentally. From a general perspective, this can be considered as a consequence of the fact that it becomes extremely difficult to extract any

useful information from the large Hilbert space.

Finally, we have conducted a proof-of-principle experiment on a real quantum hardware, which suggests that adversarial training can be a useful tool to make quantum kernel methods robust, not just against input perturbations, but also against hardware noise.

As another future perspective, it would be interesting to link the generalization capabilities of quantum kernel methods and their adversarial robustness. The generalization capabilities of the quantum-enhanced SVM classifier are defined intrinsically by the quantum embedding circuit leveraged for quantum kernel estimation, and can be bounded in several ways (Banchi *et al.* 2021, 2023; Huang *et al.* 2021; Caro *et al.* 2022). Moreover, a link between generalization and adversarial learning was recently considered in Georgiou *et al.* (2024). However, there are currently no empirical guidelines to select an appropriate quantum embedding circuit for a specific classification task.

Acknowledgements

L.B. acknowledges support from: Prin 2022 - DD N. 104 del 2/2/2022, entitled “understanding the LEarning process of QUantum Neural networks (LeQun)”, proposal code 2022WHZ5XH, CUP B53D23009530006; U.S. Department of Energy, Office of Science, National Quantum Information Science Research Centers, Superconducting Quantum Materials and Systems Center (SQMS) under the Contract No. DE-AC02-07CH11359; PNRN Ministero Università e Ricerca Project No. PE0000023-NQSTI.

A. Quantum Kernel Alignment

Aside from some specific cases, for instance where datasets to consider belong to a group (Glick *et al.* 2024), the selection of a kernel and the associated feature map is not immediate, and no general guideline is available. In a context like ours, where the quantum embedding is a parameterized circuit, looking for a “good” kernel means looking for a parameters set that enables to obtain a “good” classifier. Common metrics to evaluate the quality of a classifier, like accuracy, precision, recall, etc., do not fit well for this purpose because these are discrete metrics that do not allow to detect small improvements due to a parameters change, for example in terms of gen-

eralization, and that approach would require to perform an exhaustive search in the parameter space without any hint on regions where to search. A specialized measure that we can use is the *kernel-target alignment*. Such a measure derives directly from the *kernel alignment* (Cristianini *et al.* 2001; Wang *et al.* 2015) that is defined as:

$$A(K_1, K_2) = \frac{\langle K_1, K_2 \rangle}{\sqrt{\langle K_1, K_1 \rangle \langle K_2, K_2 \rangle}}, \quad (\text{A1})$$

where K_1 and K_2 denote the kernel matrix (Gram matrix) of two kernels $k_1(\cdot, \cdot)$ and $k_2(\cdot, \cdot)$ defined over a certain dataset, and $\langle K_1, K_2 \rangle$ is the Frobenius inner product between two matrices, which is given by

$$\langle K_1, K_2 \rangle = \sum_{i,j} k_1(x_i, x_j) k_2(x_i, x_j) \quad (\text{A2})$$

Kernel alignment measures the similarity between two kernels and we can give it a geometrical interpretation: considering K_1 and K_2 as two vectors in a bi-dimensional vector space, the kernel alignment is the cosine of the angle between the two vectors. Given that is possible to show that a kernel matrix is a positive semidefinite matrix, the kernel alignment takes values between 0 and 1, with 1 indicating maximal similarity.

The kernel-target alignment measure is defined as the kernel alignment between a kernel matrix of our interest and an ideal target kernel matrix defined as $K^t = yy^T$, which represents a kernel function that assigns to each couple of samples the product of the corresponding labels: $k^t(x_i, x_j) = y_i y_j$. It can be described as:

$$A(K, K^t) = \frac{\langle K, yy^t \rangle}{\sqrt{\langle K, K \rangle \langle yy^t, yy^t \rangle}} = \frac{y^t K y}{M \|K\|} \quad (\text{A3})$$

where M is the number of elements in the labels vector y , that is the number of samples in the dataset.

The kernel-target alignment measures how well a kernel function reproduces the behaviour of the ideal target kernel, and is characterized by some properties:

1. It is computationally efficient compared to other metrics (Chapelle *et al.* 2002). It can be computed in $O(M^2)$ time complexity.
2. It enjoys the concentration property, which means that the kernel-target alignment is concentrated around its mean value. Because of this, an empirical estimate of it is close to the true alignment value.
3. It provides theoretical basis to the generalization capabilities of a binary classifier that uses a kernel with an high mean value of the kernel-target alignment. Optimizing this alignment provides an upper bound to the generalization error (the probability a trained model will predict wrong labels for unseen test samples) of a simple classifier based on center of mass of the data classes.

To tune the quantum embedding parameters and align the associated kernel to the ideal target one we need to solve an optimization problem: find the optimal parameters that maximize the kernel-target alignment

$$\theta^* = \arg \max_{\theta} A(K_{\theta}, K^t), \quad (\text{A4})$$

where K_{θ} is the Gram matrix for the parameterized kernel $k_{\theta}(\cdot, \cdot)$.

Assuming that the kernel is differentiable, it is possible to show that kernel-target alignment is differentiable with respect to the parameters vector and therefore it is possible to use a gradient based algorithm to optimize the parameters. Clearly, since we want to maximize the alignment, we have to minimize its opposite, that means the kernel-target alignment multiplied by -1, or use a gradient ascent algorithm.

For this project we decided to exploit a slightly different method to implement the kernel alignment. In particular we followed the approach described in Glick *et al.* (2024). Instead of maximizing the kernel-target alignment, we look for the parameters set that minimize the upper boundary for the generalization error. In particular, the object function of the optimization problem to consider, coincides with the decision function of the nonlinear SVM algorithm, in the dual problem formulation:

$$F(\alpha, \theta) = \sum_i \alpha_i - \frac{1}{2} \sum_{i,j} \alpha_i \alpha_j y_i y_j k_{\theta}(x_i, x_j) \quad (\text{A5})$$

Fitting a SVM model entails the maximization of this function under constraints, as shown by Eq. (5), while optimizing for generalization requires minimizing this same function over the kernel parameters θ . This min-max problem can be interpreted as choosing a kernel among all the possible K_{θ} that minimize the SVM bound on the classification error. In terms of complexity, this metrics is less efficient than kernel-target alignment, since in addition to the evaluation of a Gram matrix in $O(M^2)$ we have also to solve the dual optimization problem for maximizing the margin of a SVM model. Nevertheless, this approach allows to reduce the boundary for the generalization error of an SVM classifier, and this is an important aspect for the purposes of this work.

B. Details of numerical results

Regarding the experiments on the kernel alignment procedure we can report some observations:

1. The objective function $F(\alpha, \theta)$ (A5) can be seen as a function enclosing a weighted version of (5) (with $\alpha_i \alpha_j$ as weights) and it is differentiable respect to both α and θ . We did some simulations to compare the use of SPSA and COBYLA as optimizers. The use of a gradient-based optimization algorithm like SPSA looks generating smaller fluctuation of the objective function compared to the use

of COBYLA. SPSA is indeed proposed as default optimizer for a kernel alignment procedure based on the qiskit’s *QuantumKernelTrainer* tool.

2. The optimization process was carried on by means of SPSA optimizer for 80 iterations, with learning rate=0.05 and perturbation=0.05 on both feature maps. While the loss of the compact quantum embedding decreases quite smoothly and stabilizes around a value of 11, the large embedding shows a rougher evolution reaching a final value of approximately 8.
3. Considering that we executed the kernel alignment on a quantum simulator without noise, we could have used a vanilla gradient descent optimizer instead of SPSA. However, with the perspective to use this same method on a real quantum hardware affected by noise, the use of a stochastic optimization algorithm is expected to be necessary to reduce non convergence issues.
4. It’s curious to observe that the property of “concentration” described in (Cristianini *et al.* 2001) in a positive sense and exploitable to obtain kernels that allow SVM-based classifiers to generalize well, it could be some how connected to the “exponential concentration” phenomenon that affects quantum kernel methods in a negative sense and that makes difficult to carry on the training of parameterized quantum kernels (Thanasilp *et al.* 2022).

Regarding the experiments on adversarial learning:

1. We generated a set of 50 adversarial examples for both QSVM classifiers based on large and compact embedding, respectively, by means of the iterative process described by (11), with $\eta = 0.01$.
2. The algorithm takes less then 50 iterations to generate an adversarial example for the compact embedding while, for the large embedding, it takes approximately 1270 iterations in the worst case.

C. Alternative technique to generate adversarial samples

To deal with a general quantum kernel we have to identify a different technique that does not require the knowledge about the gradient of the kernel. A possible approach consists on setting up an optimization problem where we use an objective function that once minimized satisfies the same goals of the adversarial learning technique for QSVM. To generate a good adversarial sample starting from an unperturbed input sample we have to satisfy two conditions simultaneously (as already mentioned in section 3):

1. To perturb an input sample x into its adversarial version x_{adv} so that its associated vector $\rho(x)$ in the

larger feature space gets shifted to $\rho(x_{adv})$ on the opposite side of the optimal decision plane defined by the QSVM classifier.

2. To keep the distance between x and x_{adv} as small as possible.

To foster the achievement of the first goal we can define a function satisfying that same condition when it gets minimized. There are clearly infinite ways to do that. One possibility is to define a function like:

$$g_1(x_{adv}) = \max(0, 1 - y_i r_{adv}) = \quad (C1)$$

$$= \max\left(0, 1 - y_i \frac{\langle w, \rho(x_{adv}) \rangle + b}{\sqrt{\langle w, w \rangle}}\right) = \quad (C2)$$

$$= \max\left(0, 1 - y_i \frac{f(x_{adv})}{\|w\|^2}\right), \quad (C3)$$

where r_{adv} is the distance of the feature vector $\rho(x_{adv})$ from the nonlinear SVM’s decision plane, defined by the tuple (w, b) , and $f(x_{adv})$ is the decision function of the SVM.

The nonlinear function (C1) takes values zero when $\rho(x_{adv})$ is, simultaneously, at a distance greater than or equal to 1 from the decision plane (w, b) and on the opposite side with respect to $\rho(x)$. Otherwise, the function takes a positive value which magnitude increases linearly while $\rho(x_{adv})$ moves toward the the side of the decision plane where $\rho(x)$ lies. Minimizing (C1) implies searching for an x_{adv} for which the SVM classifier predicts a label different from the unperturbed sample’s one.

To pursue the second goal we can define a function that has a minimum when the distance $\text{dist}(x, x_{adv})$ is minimized. For instance we can consider the squared distance:

$$g_2(x_{adv}) = \|x - x_{adv}\|_2^2 \quad (C4)$$

We can define an overall objective function for our optimization problem as a combination of the previous two functions, where we introduce some parameters that we can use to tune empirically the minimization process:

$$g(x_{adv}, \epsilon, \mu) = g_1(x_{adv})^\epsilon + \mu g_2(x_{adv}) = \quad (C5)$$

$$= \left(\max\left(0, 1 - y_i \frac{f(x_{adv})}{\|w\|^2}\right)\right)^\epsilon + \mu \|x - x_{adv}\|_2^2$$

The legitimate training sample x is considered a constant. The objective function $g(x, \epsilon, \mu)$ is a nonlinear function with respect to x_{adv} and therefore we can only aim to find local optimal values. Furthermore, considering that the QSVM’s decision function $f(x_{adv})$ is nonlinear, nothing prevents function (C5) to have one or more local/global minimums where (C1) is different from zero.

This technique to generate adversarial samples is therefore an empirical process where parameters ϵ and μ need to be tuned in a trial and error iterative process that brings to generate adversarial examples while keeping (C4) limited. Some adversarially generated samples are shown in Fig. 7.

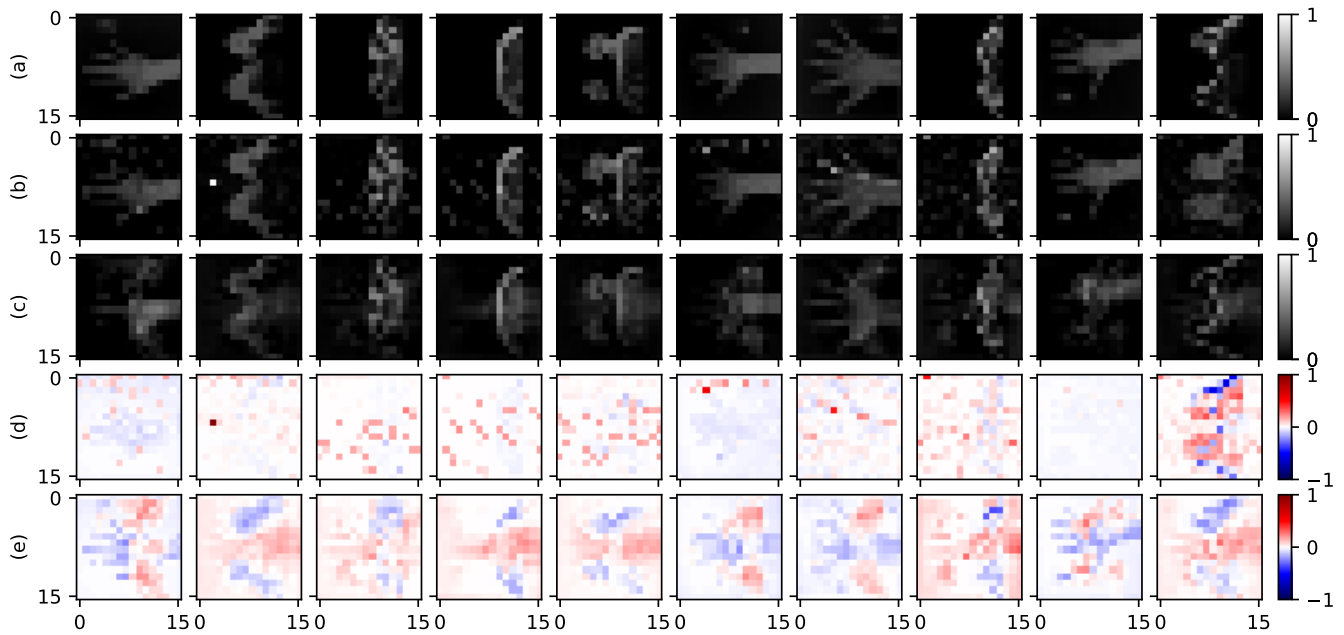


FIG. 7. Example of adversarial images generated with the alternative adversarial learning technique, with $\epsilon = 3.0$ and $0.5 \leq \mu \leq 2.0$. In each column, (a) is the original sample, (b) and (c) the corresponding adversarial examples for the large and compact feature map, respectively, (d) and (e) the perturbation that summed up to the original image generates (b) and (c), respectively.

References

- B. Biggio and F. Roli, Wild patterns: Ten years after the rise of adversarial machine learning, in *Proceedings of the 2018 ACM SIGSAC Conference on Computer and Communications Security* (2018) pp. 2154–2156.
- C. Szegedy, W. Zaremba, I. Sutskever, J. Bruna, D. Erhan, I. Goodfellow, and R. Fergus, Intriguing properties of neural networks, in *2nd International Conference on Learning Representations, ICLR 2014* (2014).
- M. Schuld, I. Sinayskiy, and F. Petruccione, An introduction to quantum machine learning, *Contemporary Physics* **56**, 172 (2015).
- S. Lu, L.-M. Duan, and D.-L. Deng, Quantum adversarial machine learning, *Physical Review Research* **2**, 033212 (2020).
- N. Liu and P. Wittek, Vulnerability of quantum classification to adversarial perturbations, *Physical Review A* **101**, 062331 (2020).
- W. Ren, W. Li, S. Xu, K. Wang, W. Jiang, F. Jin, X. Zhu, J. Chen, Z. Song, P. Zhang, *et al.*, Experimental quantum adversarial learning with programmable superconducting qubits, *Nature Computational Science* **2**, 711 (2022).
- V. Gebhart, R. Santagati, A. A. Gentile, E. M. Gauger, D. Craig, N. Ares, L. Banchi, F. Marquardt, L. Pezzè, and C. Bonato, Learning quantum systems, *Nature Reviews Physics* **5**, 141 (2023).
- Qiskit contributors, Qiskit: An open-source framework for quantum computing (2023).
- M. Schuld and F. Petruccione, *Machine learning with quantum computers* (Springer, 2021).
- N. Cristianini and J. Shawe-Taylor, *An introduction to support vector machines and other kernel-based learning methods* (Cambridge university press, 2000).
- Y. Liu, S. Arunachalam, and K. Temme, A rigorous and robust quantum speed-up in supervised machine learning, *Nature Physics* **17**, 1013 (2021).
- C.-C. Chang and C.-J. Lin, Libsvm: a library for support vector machines, *ACM transactions on intelligent systems and technology (TIST)* **2**, 1 (2011).
- V. Havlíček, A. D. Córcoles, K. Temme, A. W. Harrow, A. Kandala, J. M. Chow, and J. M. Gambetta, Supervised learning with quantum-enhanced feature spaces, *Nature* **567**, 209 (2019).
- W. Li, X. Liu, A. Yan, and J. Yang, Kernel-based adversarial attacks and defenses on support vector classification, *Digital Communications and Networks* **8**, 492 (2022).
- S. Thanasilp, S. Wang, and Z. Holmes, Exponential concentration and untrainability in quantum kernel methods, *arXiv preprint arXiv:2208.11060* (2022).
- K. Mitarai, M. Negoro, M. Kitagawa, and K. Fujii, Quantum circuit learning, *Physical Review A* **98**, 032309 (2018).
- L. Banchi and G. E. Crooks, Measuring analytic gradients of general quantum evolution with the stochastic parameter shift rule, *Quantum* **5**, 386 (2021).
- L. Banchi, Robust quantum classifiers via nisq adversarial learning, *Nature Computational Science* **2**, 699 (2022).
- L. Banchi, J. Pereira, and S. Pirandola, Generalization in quantum machine learning: A quantum information stand-

point, PRX Quantum **2**, 040321 (2021).

L. Banchi, J. L. Pereira, S. T. Jose, and O. Simeone, Statistical complexity of quantum learning, arXiv preprint arXiv:2309.11617 (2023).

H.-Y. Huang, M. Broughton, M. Mohseni, R. Babbush, S. Boixo, H. Neven, and J. R. McClean, Power of data in quantum machine learning, Nature communications **12**, 2631 (2021).

M. C. Caro, H.-Y. Huang, M. Cerezo, K. Sharma, A. Sornborger, L. Cincio, and P. J. Coles, Generalization in quantum machine learning from few training data, Nature communications **13**, 4919 (2022).

P. Georgiou, S. T. Jose, and O. Simeone, Adversarial quantum machine learning: An information-theoretic generalization analysis, arXiv preprint arXiv:2402.00176 (2024).

J. R. Glick, T. P. Gujarati, A. D. Corcoles, Y. Kim, A. Kandala, J. M. Gambetta, and K. Temme, Covariant quantum kernels for data with group structure, Nature Physics , 1 (2024).

N. Cristianini, J. Shawe-Taylor, A. Elisseeff, and J. Kandola, On kernel-target alignment, Advances in neural information processing systems **14** (2001).

T. Wang, D. Zhao, and S. Tian, An overview of kernel alignment and its applications, Artificial Intelligence Review **43**, 179 (2015).

O. Chapelle, V. Vapnik, O. Bousquet, and S. Mukherjee, Choosing multiple parameters for support vector machines, Machine learning **46**, 131 (2002).